www.springer.com/41230
https://doi.org/10.1007/s41230-022-1157-4

Numerical simulation on fluid flow behavior during 3-dimensional dendrite growth with random preference angle

Qi Wang, Ke-jie Feng, Shi-jie Zhang, Chen-yu Li, and *Ri Li

School of Materials Science and Engineering, Hebei University of Technology, Tianjin 300401, China

Abstract: The flow behavior of three-dimensional (3D) dendrite growth with random preferred angle under natural convection was studied by using the Lattice Boltzmann-Cellular Automata (LB-CA) method with dynamic and static grids. In this model, the temperature field, flow field and solute field calculated by Lattice Boltzmann method (LBM) and dendrite growth calculated by CA method were carried out in static and dynamic grids respectively, and the coupling between LBM and CA was performed by interpolation of calculation parameters between dynamic and static grids. Results show that the asymmetry of solid phase distribution makes the streamline distribution more complex. At the initial stage of multiple dendrites growth, the fluid flow is relatively free. When dendrites grow close to each other, the fluid flow is blocked and can only flow along the gap between dendrites. During the wall equiaxed-columnar-central equiaxed crystals transformation (ECET) process, dense eddy current is formed at the wall equiaxed crystals at first. Then, when the wall equiaxed crystals gradually develop into columnar crystals, the eddy current moves with the solid-liquid interface. When the central equiaxed crystals are formed, the eddy current at the front of the columnar crystals gradually disappears. New eddies appear as the central equiaxed crystal grows.

Keywords: two sets of grids; randomly select; preference angle; three dimensional LB-CA model; fluid flow

CLC numbers: TP391.9 **Document code:** A **Article ID:** 1672-6421(2022)05-387-08

1 Introduction

With the rapid development of computer technology, using numerical simulation method to study dendrite growth process is more and more favored by scholars. To simulate the microstructure evolution process of materials, appropriate research methods need to be adopted, which should not only improve the calculation efficiency as much as possible, but also ensure the calculation accuracy. Lattice Boltzmann Method (LBM) is a mesoscopic fluid calculation method developed in recent years. Compared with several other fluid calculation methods [1-2], LBM has good stability, can calculate complex fluid boundaries, and its algorithm is simple [3-4]. Especially, it can efficiently calculate the melt flow between dendrites, which is difficult to achieve by traditional continuity methods such as finite volume method (FVM), finite element method (FEM) and finite difference method (FDM). Cellular automata (CA) has a physical background in calculating dendrite growth, and the program is relatively simple. At present, it has become one of the main methods for alloy solidification structure simulation calculation [5-7]. Coupling the above two methods can give full play to their advantages and have great potential in solidification structure simulation.

At present, many scholars used CA method to study 3D dendrite growth. Brown et al. [8-9] established a coupling model of 3D CA and FDM to calculate the eutectic growth. Wang et al. [10] predicted the primary dendrite arm spacing by coupling 3D CA with FDM, and simulated the evolution process of equiaxed and columnar crystals. Pan et al. [11] established a sharp interface model to simulate the growth morphology of 3D equiaxed crystals with different growth angles. Xu et al. [12] established a 3D CA model to simulate the solidification process of ingot, which improved the calculation efficiency through macro and micro coupling, and the calculation results were also consistent with the experimental results. Jiang et al. [13]

***Ri Li**

Born in 1966, Professor. His research interest mainly focuses on material processing CAD/CAE.

E-mail: sdzllr@163.com

Authors Qi Wang and Ke-jie Feng contributed equally to this work.

Received: 2021-08-16; Accepted: 2022-03-15

proposed a 3D model that can calculate the dendritic morphology evolution of the alloy by combining CA and FDM, which can accurately calculate the microstructure evolution process of the alloy during solidification. Zhang et al. [14] established a 3D CA model to simulate the grain evolution. The correctness of the model was verified by comparison with the theoretical predictions of binary and ternary alloys, and the effect of the interaction between several alloy elements on grain growth was studied. Wei et al. [15] presented a limited neighbor solid fraction method to reduce the mesh induced anisotropy, and established a 3D adaptive mesh refinement CA model to simulate the morphology of 3D equiaxed dendrites of pure materials. Chen et al. [16] established an improved CA model, which can calculate the growth of equiaxed grains of ternary aluminum alloys, and the calculated results are consistent with the experimental results. Pian et al. [17] established a model that can calculate the regular growth of 3D dendrites. The calculation results of the model are consistent with the actual situation. Cheng et al. [18] developed a quantitative CA model to calculate the dendrite morphology evolution during solidification of 3D ternary alloys. The model can accurately calculate the solute distribution and morphology of equiaxed dendrites and columnar crystals during solidification, and can also simulate the effect of the third component concentration on the grain growth process.

The above 3D numerical simulation of dendrites is limited to the free growth of several equiaxed dendrites under pure thermal diffusion and solute diffusion condition, and the flow behavior of fluid between dendrites is not involved. In the actual solidification process, the growth of dendrite is accompanied by the release of latent heat and the discharge of solute, which will cause density difference in the melt from two aspects of temperature and concentration, and then lead to natural convection in the melt, which in turn affect the growth of dendrite. Therefore, fluid flow is one of the important factors affecting the growth of dendrite. The study of fluid flow pattern in dendrite growth process is of great significance to deeply understand the formation mechanism of microstructure.

In this study, a LB-CA coupling model based on two sets of grids was constructed. LBM was used to calculate the macro field transmission in the static grid and CA method was used to calculate the dendrite growth in the dynamic grid. The fluid flow behavior during dendrite growth with random preferred growth orientation was studied by using this model.

2 Material and methods

Al-4.7wt.% Cu alloy is selected as the simulation material, and its calculated thermophysical parameters are shown in Table 1.

Table 1: Physical properties of Al-4.7wt.%Cu alloy

Physical parameter	Symbol	Value
Liquidus temperature	T_L (K)	917
Solidus temperature	T_S (K)	821
Liquidus slope	m [K(wt.%)$^{-1}$]	−3.44
Thermal diffusivity	α (W·m^{-1}·K^{-1})	3×10^{-8}
Interface anisotropy coefficient	ε	0.05
Diffusivity in liquid	D (m^2·s^{-1})	3.0×10^{-9}
Partition coefficient	k	0.145
Kinematic viscosity	v (m^2·s^{-1})	9×10^{-9}

2.1 LBM model

The D3Q15 model of LBM was used to calculate the macroscopic field. The evolution equation of flow field distribution function is [19]:

$$f_i(\boldsymbol{x}+\boldsymbol{e}_i\Delta t,t+\Delta t)-f_i(\boldsymbol{x},t)=\frac{1}{\tau_f}(f_i^{\mathrm{eq}}(\boldsymbol{x},t)-f_i(\boldsymbol{x},t))+F_i \quad (1)$$

where $f_i(\boldsymbol{x},t)$ represents the probability of particles appearing in time t and position $\boldsymbol{x}$, which is called the distribution function. $f_i^{\mathrm{eq}}(\boldsymbol{x},t)$ represents the equilibrium distribution function, Δt represents the time step, $\boldsymbol{e}_i$ represents the particle velocity, and τ_f represents the flow field relaxation time. $f_i^{\mathrm{eq}}(\boldsymbol{x},t)$ and τ_f can be obtained from Eqs. (2) and (3):

$$f_i^{\mathrm{eq}}(\boldsymbol{x},t)=\omega_i\rho\left(1+3\frac{\boldsymbol{e}_i\cdot\boldsymbol{u}}{c^2}+\frac{9}{2}\frac{(\boldsymbol{e}_i\cdot\boldsymbol{u})^2}{c^4}-\frac{3}{2}\frac{(\boldsymbol{u}\cdot\boldsymbol{u})}{c^2}\right) \quad (2)$$

$$\tau_f=3v/(c^2\Delta t)+1/2 \quad (3)$$

where c is the lattice velocity, ω_i is the weight coefficient, ρ is the density, $\boldsymbol{u}$ is the velocity, v is the fluid viscosity.

F_i is the external force source term, which represents the interaction force between fluids in natural convection, can be obtained by Eq. (4) :

$$F_i=\omega_i\left(1-\frac{1}{2\tau_f}\right)\left[\frac{3(\boldsymbol{e}_i-\boldsymbol{u})}{c^2}+\frac{9\boldsymbol{e}_i\cdot\boldsymbol{u}}{c^4}\right]\boldsymbol{F}\cdot\Delta t \quad (4)$$

According to the Boussinesq approximation, the buoyancy $\boldsymbol{F}$ can be calculated by Eq. (5):

$$\boldsymbol{F} = \boldsymbol{g}\rho_0\beta_T(T-T_0) + \boldsymbol{g}\rho_0\beta_C(C-C_0) \quad (5)$$

where ρ_0 represents the initial density of the fluid, T_0 represents the initial temperature, T represents the current temperature, C_0 represents the initial concentration, C represents the current concentration, β_T and β_C represents the volume expansion coefficient of the temperature change and the concentration change respectively, $\boldsymbol{g}$ represents the gravity acceleration.

In the calculation of temperature field and concentration field, the distribution functions of temperature, $h_i(\boldsymbol{x},t)$, and concentration, $g_i(\boldsymbol{x},t)$ can be calculated by Eq. (6) and Eq. (7):

$$h_i(\boldsymbol{x}+\boldsymbol{e}_i\Delta t, t+\Delta t) = h_i(\boldsymbol{x},t) + \frac{1}{\tau_\alpha}(h_i^{eq}(\boldsymbol{x},t) - h_i(\boldsymbol{x},t)) + H_i \quad (6)$$

$$g_i{=}(\boldsymbol{x}+\boldsymbol{e}_i\Delta t, t+\Delta t) = g_i(\boldsymbol{x},t) + \frac{1}{\tau_D}(g_i^{eq}(\boldsymbol{x},t) - g_i(\boldsymbol{x},t)) + G_i \quad (7)$$

The equilibrium distribution function corresponding to temperature and concentration can be calculated by Eq. (8) and Eq. (9), respectively:

$$h_i^{eq}(\boldsymbol{x},t) = \omega_i T\left(1 + 3\frac{\boldsymbol{e}_i\cdot\boldsymbol{u}}{c^2} + \frac{9}{2}\frac{(\boldsymbol{e}_i\cdot\boldsymbol{u})^2}{c^4} - \frac{3}{2}\frac{(\boldsymbol{u}\cdot\boldsymbol{u})}{c^2}\right) \quad (8)$$

$$g_i^{eq}(\boldsymbol{x},t) = \omega_i C\left(1 + 3\frac{\boldsymbol{e}_i\cdot\boldsymbol{u}}{c^2} + \frac{9}{2}\frac{(\boldsymbol{e}_i\cdot\boldsymbol{u})^2}{c^4} - \frac{3}{2}\frac{(\boldsymbol{u}\cdot\boldsymbol{u})}{c^2}\right) \quad (9)$$

In Eq. (6) and Eq. (7), the values of temperature field relaxation time τ_α and concentration field relaxation time τ_D can be calculated by corresponding thermal diffusion coefficient α and solute diffusion coefficient D, respectively:

$$\tau_\alpha = 3\alpha/(c^2\Delta t) + 1/2 \quad (10)$$

$$\tau_D = 3D/(c^2\Delta t) + 1/2 \quad (11)$$

H_i and G_i in Eq. (6) and Eq. (7) represent concentration and temperature source term, respectively, and their values can be calculated by:

$$G_i = \omega_i C_l(1-k)\Delta f_s \quad (12)$$

$$H_i = \omega_i \Delta f_s L/c_p \quad (13)$$

where, C_l represents the liquid phase composition, k represents the equilibrium distribution coefficient, Δf_s is the increase of solid fraction of an interface cell, L represents the solidification latent heat, c_p represents the specific heat capacity.

The macroscopic physical quantity can be calculated by adding the corresponding distribution function:

$$\rho = \sum_{i=0}^{14} f_i \quad (14)$$

$$\boldsymbol{u} = \left(\sum_{i=0}^{14}\boldsymbol{e}_i f_i + \boldsymbol{F}\cdot\Delta t/2\right)/\rho \quad (15)$$

$$T = \sum_{i=0}^{14} h_i(\boldsymbol{x},t) \quad (16)$$

$$C = \sum_{i=0}^{14} g_i(\boldsymbol{x},t) \quad (17)$$

All boundaries of the flow field were treated by the non slip bounce back. For the concentration field, the boundary of the computational domain was the non-diffusion boundary, and the solid-liquid boundary was treated by bounce back. For the temperature field, the boundary of the simulation region was treated by non-equilibrium extrapolation, and it was assumed that the thermal conductivity of the solid phase and the liquid phase were the same.

2.2 CA model

The solute diffusion model proposed by Pan et al. [11] was used for the calculation of grain morphology evolution. The Δf_s of growth grid can be calculated by:

$$\Delta f_s = \left(C_l^{eq} - C_l\right)/\left[C_l^{eq}(1-k)\right] \quad (18)$$

where, C_l^{eq} represents the equilibrium solute concentration of the cell, can be calculated as:

$$C_l^{eq} = C_0 + \left(T - T^{eq}\right)/m + wmc\cdot\Gamma/m \quad (19)$$

where, T^{eq} represents the equilibrium liquidus temperature at the concentration of C_0, m represents the slope of the liquid line of the alloy, Γ represents the Gibbs-Thomson coefficient, and wmc represents the weighted mean curvature at a 3D scale, the value of which can be calculated by:

$$\begin{aligned} wmc = {} & (3\varepsilon-1)\left(\partial n_x/\partial x + \partial n_y/\partial y + \partial n_z/\partial z\right) \\ & +12Q\varepsilon\left(\partial n_x/\partial x + \partial n_y/\partial y + \partial n_z/\partial z\right) \\ & +12\varepsilon\left(n_x\cdot\partial Q/\partial x + n_y\cdot\partial Q/\partial y + n_z\cdot\partial Q/\partial z\right) \\ & -48\varepsilon\left(n_x^2\cdot\partial n_x/\partial x + n_y^2\cdot\partial n_y/\partial y + n_z^2\cdot\partial n_z/\partial z\right) \end{aligned} \quad (20)$$

where, ε represents the anisotropy coefficient of interface energy, n_x, n_y, n_x and Q can be calculated by Eq. (21) to Eq. (25):

$$n_x = \left(\partial f_s/\partial x\right)/\left|\nabla f_s\right| \quad (21)$$

$$n_y = \left(\partial f_s/\partial y\right)/\left|\nabla f_s\right| \quad (22)$$

$$n_z = \left(\partial f_s/\partial z\right)/\left|\nabla f_s\right| \quad (23)$$

$$Q = n_x^4 + n_y^4 + n_z^4 \quad (24)$$

$$\left|\nabla f_s\right| = \sqrt{(\partial f_s/\partial x)^2 + (\partial f_s/\partial y)^2 + (\partial f_s/\partial z)^2} \quad (25)$$

where f_s is the solid fraction of an interface cell.

2.3 Nucleation model

The continuous nucleation model based on Gaussian distribution proposed by Rappaz et al. [20] was selected as the nucleation part of this study. This model is widely used in the numerical simulation in foundary and other fields [21-22].

The functional relationship between nucleation rate and undercooling in the continuous nucleation model can be expressed as:

$$\frac{\mathrm{d}n}{\mathrm{d}(\Delta T)}=\frac{n_{\max}}{\sqrt{2\pi}\Delta T_{\sigma}}\exp\left[-\frac{1}{2}\left(\frac{\Delta T-\Delta\overline{T}}{\Delta T_{\sigma}}\right)^{2}\right] \tag{26}$$

where n represents the melt nucleation density; $n_{\max}$ represents the maximum nucleation density; ΔT is the undercooling; ΔT_{σ} is the standard variance undercooling; $\Delta\overline{T}$ is the average of nucleation undercooling. The nucleation density can be obtained by integrating the above formula:

$$n(\Delta T)=\int_{0}^{\Delta T}\frac{\mathrm{d}n}{\mathrm{d}(\Delta T)}\mathrm{d}(\Delta T) \tag{27}$$

2.4 Two sets of grid methods

The whole computing domain was divided into static grids, which are in the absolute coordinate system; each dendrite was set with its own dynamic grid, which was in the dynamic coordinate system, and the direction of the dynamic coordinate system was consistent with the growth direction of the dendrite. Therefore, dendrites always grow regularly in their dynamic coordinate system, and the size of dynamic grid changes dynamically with the growth of dendrites [23].

The temperature field, solute field and flow field were calculated by LBM in the absolute coordinate system, the calculation results were transformed into the dynamic grid in the dynamic coordinate system by interpolation method, and then the dendrite growth was calculated by CA method. Dendrites grow regularly in dynamic coordinate system without considering mesh anisotropy. In one time step, after calculating the dendrite growth in the dynamic coordinate system of each dendrite, the calculation results were converted to the static grid of the absolute coordinate system for the next cycle calculation. LBM and CA were calculated independently in dynamic and static grids, respectively, and the data exchange was realized by coordinate transformation and interpolation calculation.

Coordinate conversion was realized by coordinate rotation matrices R_1, R_2 and R_3. The three coordinate rotation matrices are respectively shown in Eq. (28)–Eq. (30):

$$R_1=\begin{bmatrix}\cos(\mathrm{angle}\_z) & -\sin(\mathrm{angle}\_z) & 0\\ \sin(\mathrm{angle}\_z) & \cos(\mathrm{angle}\_z) & 0\\ 0 & 0 & 1\end{bmatrix} \tag{28}$$

$$R_2=\begin{bmatrix}\cos(\mathrm{angle}\_y) & 0 & \sin(\mathrm{angle}\_y)\\ 0 & 1 & 0\\ -\sin(\mathrm{angle}\_y) & 0 & \cos(\mathrm{angle}\_y)\end{bmatrix} \tag{29}$$

$$R_3=\begin{bmatrix}1 & 0 & 0\\ 0 & \cos(\mathrm{angle}\_x) & -\sin(\mathrm{angle}\_x)\\ 0 & \sin(\mathrm{angle}\_x) & \cos(\mathrm{angle}\_x)\end{bmatrix} \tag{30}$$

where, angle_x, angle_y and angle_z are the preferred angle of the dendrite.

3 Results and analysis

3.1 Streamline around single dendrite and three dendrites

The simulation area was divided into 140×140×140 cells, the undercooling was set to 7 K, and the static grid size was 0.5 μm. The dynamic mesh size was also 0.5 μm. The initial concentration in the simulation area was C_0, a crystal seed was placed in the center of the calculation area, the angle of the seed was π/4, π/4 and 5π/4, respectively, and the initial concentration of the seed was kC_0. Figure 1 shows the distribution of streamlines around the growth of a single dendrite (some streamlines are selected for analysis). Due to the discharge of solute and latent heat from the dendrite solid-liquid interface to the liquid phase during solidification, natural convection is formed.

It can be seen from Fig. 1 that there are vortices near the tip of the solidified dendrite, and there are through flows between the main dendrite arms. This is because at the dendrite tip, there is a large space for fluid free movement, which is conducive to the formation of vortices; while between the dendrite arms, the vortices cannot be expanded due to the obstruction of the dendrite arms, so through flow is formed.

Figure 2 shows the cross-section of concentration field [Fig. 2(a)], temperature field [Fig. 2(b)] and flow field [Fig. 2(c)] of three adjacent dendrites at a certain time. The simulation area was divided into 100×100×100 cells, other conditions were the same as those for single dendrite. Three seeds were placed in the computing domain, the coordinates of which were (50, 50, 50), (60, 50, 60) and (60, 60, 60), respectively, and the angle_ x, angle_ y, angle_ z were π/4, π/4, π/4; π/3, π/3, π/3;

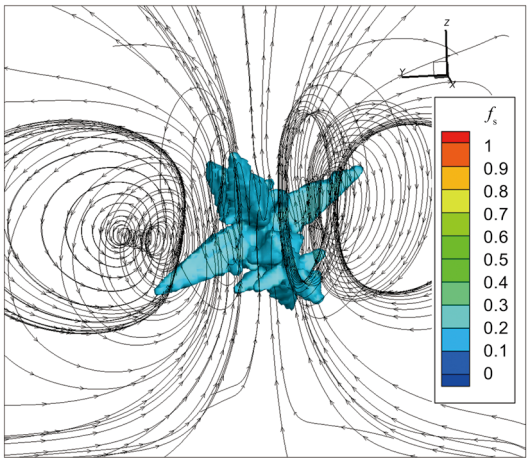

Fig. 1: Streamline distribution of single dendrite

π/7, π/3, π/6, respectively.

The difference in density is the cause of natural convection, so the solute and temperature fields were analyzed at first. In Fig. 2(a), Zone 1 represents the cross-section of dendrites, Zone 2 represents the liquid phase between dendrites, Zone 3 represents the liquid phase at the front of the solid-liquid interface facing the melt, and Zone 4 represents the liquid phase in other parts of the calculation domain. It can be seen that the concentration of Zone 1 is less than 1%, Zone 2 is about 5.5%, Zone 3 is about 5%, and Zone 4 is about 4.7%, which is the initial concentration of liquid phase. In Fig. 2(a), the concentration of solid phase is the lowest in the whole section, followed by the initial concentration of liquid phase, and the concentration around the solid phase is the highest, and the concentration of the liquid phase between dendrites is higher than that in the area where dendrites facing the liquid phase, which is consistent with the concentration distribution law during dendrite growth.

Figure 2(b) shows the cross section of the temperature field. Zone 1 represents the liquid phase in the calculation domain and Zone 2 represents the solid phase region and the liquid phase region between dendrites.

Since this model assumes that the temperature diffusion coefficients of solid and liquid phases are the same, there is no obvious gradient between dendrites as shown in Fig. 2(b). When the liquid phase solidifies, the latent heat releases to the surrounding region. The temperature gradient between Zone 2 and Zone 1 can be seen in Fig. 2(b), which is the result of the release of latent heat to the outer melt.

Due to the asymmetric distribution of the solid phase in the calculation domain, the release of latent heat and solute is uneven, therefore, the internal temperature field of the solid phase is uneven, and there are some parts with high temperature, so there are some spots with relatively high temperature in Zone 2. The streamline in the simulation area is asymmetric, and the fluid flow mode is more complex than that of single dendrites, as shown in Fig. 2(c).

Figure 2(c) shows the streamline distribution during the growth of three adjacent dendrites. It can be seen that, similar to the single dendrite, there is obvious vortex flow near the dendrite tip. In the vertical direction, the flow between dendrites is formed, which is limited by the dendrite arm. In addition, in Fig. 2(c), the three dendrite tips at the bottom grow upstream, the three dendrite tips at the top grow downstream, and the solute is transported along the flow direction. Therefore, the solute is enriched at the downstream tip. As a result, the dendrite growth at the upstream tip is faster than that at the downstream tip.

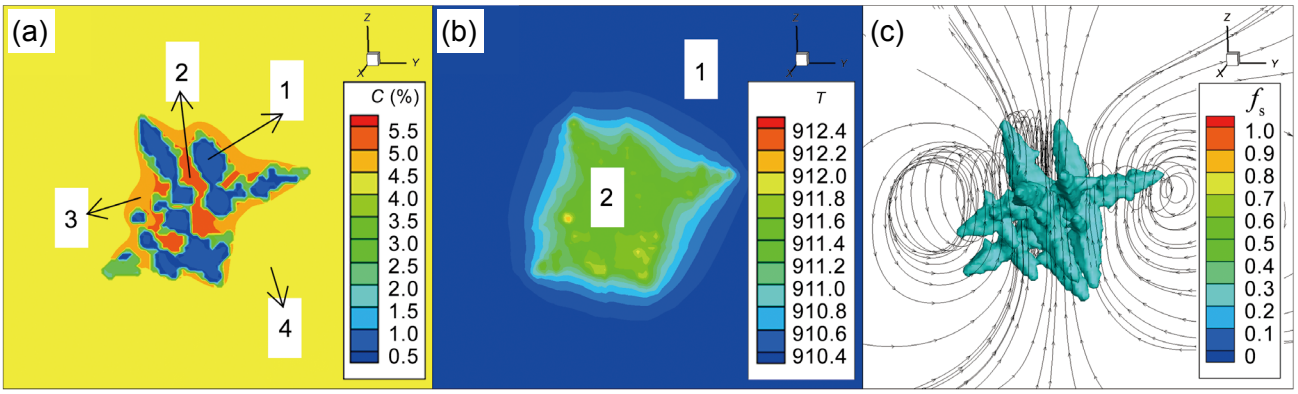

Fig. 2: Cross section of macro field calculation results of three dendrites: (a) concentration field; (b) temperature field; (c) partial streamline

3.2 Changes of streamline during multiple dendrite growth

The simulation domain was divided into 80×80×80 cells. The number and location of crystal seeds were calculated by the continuous nucleation model proposed by Rappaz et al [20]. The preferred angle of each seed was randomly selected, and the other conditions were the same as the simulation conditions in Section 3.1.

Figure 3 shows the solid phase and streamline distribution in the calculation domain. It can be seen that the dendrites form a complex 3D skeleton network structure during the growth of multiple seeds, which hinders and limits the flow of melt, but the streamline passing between dendrites can still be observed, which is difficult to be calculated by traditional fluid calculation methods such as FVM. In Fig. 3(a), there is still a certain distance between dendrites, so the melt flow near each dendrite is relatively smooth, and obvious dense vortex at the tip of dendrite can be seen. When the dendrites continue to grow to contact, as shown in Fig. 3(b), the space available for liquid flow becomes narrow, the melt can only flow along the channels between dendrites that have not yet solidified, and the number of vortices is greatly reduced.

3.3 Changes of streamline during ECET process

When the ingot begins to solidify, under the cooling effect of the wall, fine equiaxed crystals will be formed on the wall, and then equiaxed crystals will compete to grow to form columnar crystal region. With the continuous development of columnar crystal region, equiaxed crystal will generally be formed at the front. This section studies the evolution process of melt flow in the above equiaxed-columnar-central equiaxed crystals transformation (ECET) process. The calculation

domain was divided into 40×40×40 cells, with y=0 as the only heat dissipation surface, the heat transfer coefficient of this surface was set as 800 W·m^{-2}·K^{-1}, and the other surfaces were adiabatic surfaces. Due to the limitation of calculation capacity, the position and spacing of wall seeds were preset on the heat dissipation surface, and the spacing of seed in X and Z directions of the heat dissipation surface was 2.5 μm. The continuous nucleation model was used to calculate the nucleation in the melt in the calculation domain. The initial undercooling of the liquid phase was set to 4 K, and the other calculation parameters remained unchanged.

Figures 4(a)–(h) show the flow field evolution process of ECET process in the calculation domain. At the initial stage of calculation, as shown in Fig. 4(a), near the y=0 surface, equiaxed crystals grow under the cooling of the heat dissipation surface, and the grains contact with each other. At this time, due to the solute discharge and latent heat release during solidification, dense vortex clusters are formed at the front of the solid-liquid interface, while the melt far away from the solid-liquid interface does not form vortex, because there is no obvious solute gradient and temperature gradient here. With the continuous growth of equiaxed crystal group, as shown in Figs. 4(b)–(d), the solid phase covers the whole heat dissipation surface at y=0. Several equiaxed crystals win in the competitive growth and become columnar crystals. The overall size of the solid-liquid interface increases and moves towards the positive direction of the Y axis. The eddy current scale also increases with the spread of the solid phase, but the streamline

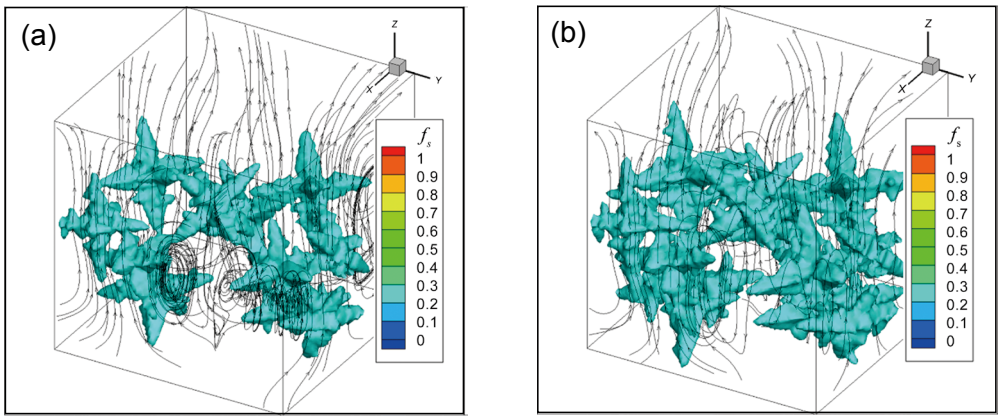

Fig. 3: Streamline distribution during multiple dendrite growth: (a) 7.5 ms; (b) 10 ms

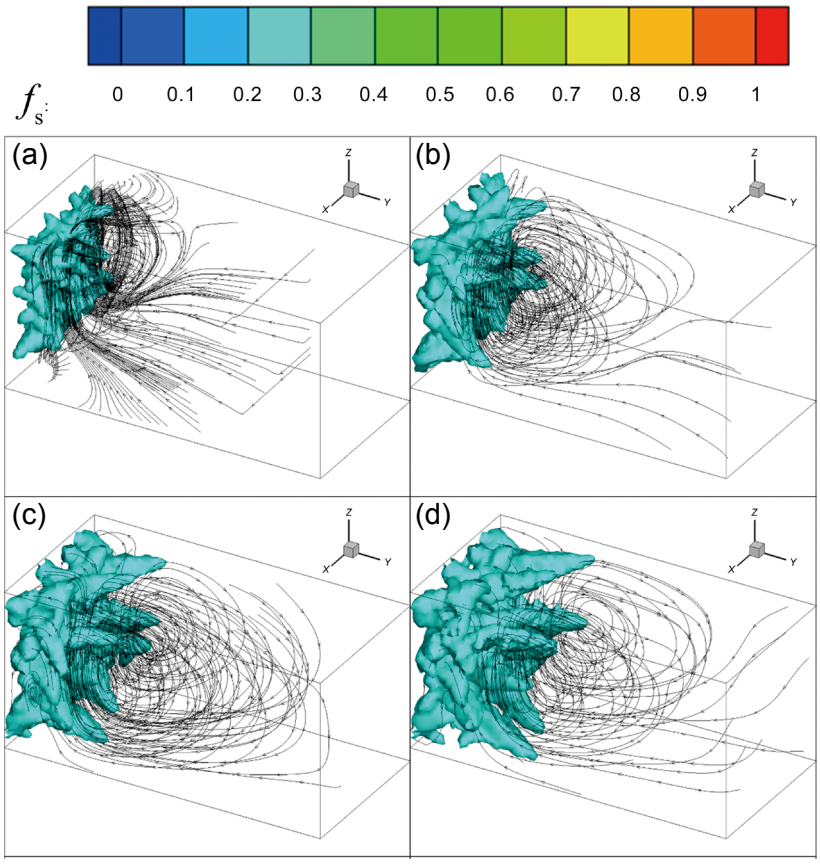

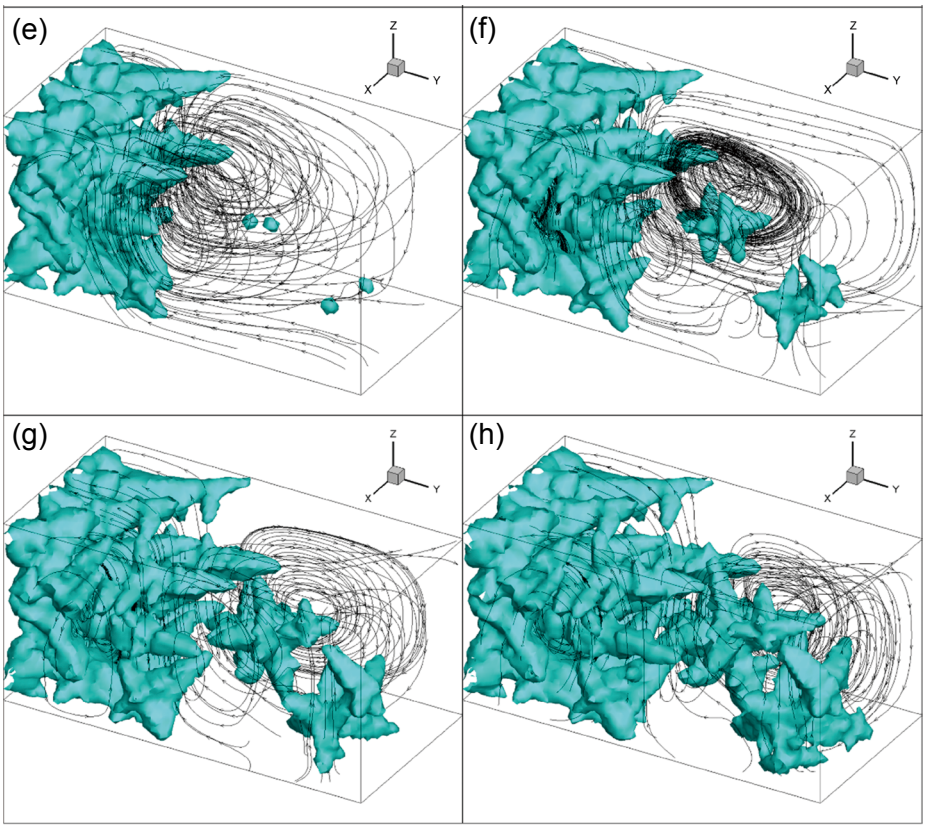

Fig. 4: Streamline distribution in calculation domain at different simulation times: (a) 2.5 ms; (b) 5 ms; (c) 7.5 ms; (d) 10 ms; (e) 12.5 ms; (f) 15 ms; (g) 17.5 ms; (h) 20 ms

becomes sparse than that in Fig. 4(a). The position of the eddy current in the calculation domain also moves steadily with the advance of the solid-liquid interface. When solidification proceeds to Fig. 4(e), equiaxed crystals appear in the front of columnar crystals, but the scale of these seeds is still very small, which is not enough to have a significant impact on the overall fluid. With the continuous progress of solidification, as shown in Figs. 4(f)–(h), new equiaxed crystals continue to form at the front of columnar crystals, and continue to grow together with the previously formed equiaxed crystals. Some equiaxed crystals are in contact with columnar crystals [Fig. 4(g)], and then adhere to them [Fig. 4(h)].

It can be observed from (f), (g) and (h) in Fig. 4 that with the coarsening and close combination of columnar crystals and the growth and expansion of equiaxed crystal region at the front of columnar crystals, the original vortex at the front of columnar crystal region gradually disappears, the streamline becomes sparse; and new eddy current regions are formed around equiaxed crystals. These flow processes are conducive to the homogenization of temperature field and concentration field. The columnar crystal and the eddy current flow at its front are the main reasons for the formation of A-type segregates in ingots [24]. Therefore, the calculation and analysis of flow during solidification is of great significance to further study the formation mechanism of macro segregation of ingot from a 3D perspective. The future work will further analyze the evolution process of solute distribution in solidification ECET process by natural convection from a 3D perspective.

4 Conclusions

On the basis of establishing a 3D LB-CA coupling model based on two sets of grids, taking Al-4.7wt.% Cu alloy as an example, the evolution process of fluid flow in the growth process of single dendrite, three dendrites, multiple dendrites and ECET process was simulated and studied. The following conclusions are obtained:

(1) In the case of single dendrite, the fluid is easy to form vortex flow near the dendrite tip, while the flow between the main dendrite arms is mainly through flow.

(2) In the process of multi dendrites growth, vortex flow can be formed between dendrites before dendrites contact, and fluid can also flow between dendrites. With the dendrites contacting each other, the region for fluid flow gradually becomes narrow, and the vortex gradually disappears, the fluid can only flow between dendrites.

(3) In the process of ECET, dense eddy currents are formed near the equiaxed crystal layer at the initial stage of wall equiaxed crystal growth. When the equiaxed crystals on the wall gradually compete to grow to form columnar crystal region, the dense eddy current becomes larger and moves to the central region with the continuous progress of the solid-liquid interface. When equiaxed crystals are formed in the front of columnar crystals, with the gradual growth of equiaxed crystals, the eddy current in the front of columnar crystals gradually disappears, and new eddy currents are generated between equiaxed crystals. As the solidification continues, the flow gradually becomes sparse.

Acknowledgements

This work was financially supported by the National Natural Science Foundation of China (Nos. 51475138 and 51975182).

References

[1] Wang W L, Luo S, Zhu M Y. Dendritic growth of high carbon iron-based alloy under constrained melt flow. Computational Materials Science, 2014, 95: 136–148.
[2] Zhang X F, Zhao J Z. Effect of forced flow on three dimensional dendritic growth of Al-Cu alloys. Acta Metallurgica Sinica, 2012, 48(5): 615–620. (In Chinese)
[3] Miller W, Succi S, Mansutti D. Lattice Boltzmann model for anisotropic liquid-solid phase transition. Physical Review Letters, 2001, 86(16): 3578–3581.
[4] Yin H, Felicelli S D, Wang L. Simulation of a dendritic microstructure with the lattice Boltzmann and cellular automaton methods. Acta Materialia, 2011, 59(8): 3124–3136.
[5] Eshraghi M, Felicelli S D, Jelinek B. Three dimensional simulation of solutal dendrite growth using lattice Boltzmann and cellular automaton methods. Journal of Crystal Growth, 2012, 354(1): 129–134.
[6] Beltran-Sanchez L, Stefanescu D M. A quantitative dendrite growth model and analysis of stability concepts. Metallurgical & Materials Transactions A, 2004, 35(8): 2471–2485.
[7] Shan B W, Lin X, Wei L, et al. A New growth kinetics in simulation of dendrite growth by cellular automaton method. Advanced Materials Research, 2007, 26–28: 957–962.
[8] Spittle J A, Brown S G K. A 3D cellular automaton model of coupled growth in two component systems. Acta Metallurgica et Materialia, 1994, 42(6): 1811–1815.
[9] Brown S G R, Bruce N B. A 3-dimensional cellular automaton model of 'free' dendritic growth. Scripta Metallurgica et Materialia, 1995, 32(2): 241–246.
[10] Wang W, Lee P D, Mclean M. A model of solidification microstructures in nickel-based superalloys: Predicting primary dendrite spacing selection. Acta Materialia, 2003, 51: 2971–2987.
[11] Pan S Y, Zhu M F. A three-dimensional sharp interface model for the quantitative simulation of solutal dendritic growth. Acta Materialia, 2010, 58(1): 340–352.
[12] Xu L, Guo H M. Simulation on solidificatioin of aluminum alloy basedon modified 3-D model. Hot Working Technology, 2011, 40(5): 1–8. (In Chinese)
[13] Jiang H X, Zhao J Z. A three-dimensional cellular automation simulation for dendritic growth. Acta Metallurgica Sinica, 2011, 47(9): 1099–1104. (In Chinese)
[14] Zhang X F, Zhao J Z, Jiang H X, et al. A three-dimensional cellular automaton model for dendritic growth in multi-component alloys. Acta Materialia, 2012, 60(5): 2249–2257.
[15] Wei L, Lin X, Wang M, et al. Orientation selection of equiaxed dendritic growth by three-dimensional cellular automaton model. Physica B, 2012, 407(13): 2471–2475.
[16] Chen R, Xu Q Y, Liu B C. A midified cellular automaton model for the quantitative prediction of equiaxed and columnar dendritic growth. Journal of Materials Science & Technology, 2014, 30(12): 1311–1320.
[17] Pian S, Zhang Z, Bao Y C, et al. Simulation of dendrite morphology and composition distribution of Al-4.7%Cu alloy based on three dimensional LBM-CA model. Materials Reports, 2017, 31(20): 140–146. (In Chinese)
[18] Cheng G, Ridgeway C D, Luo A A. Examination of dendritic growth during solidification of ternary alloys via a novel quantitative 3D cellular automaton model. Metallurgical and Materials Transactions B, 2019, 50(1): 123–135.
[19] Sun D K, Zhu M F, Pan S Y, et al. Lattice Boltzmann modeling of dendritic growth in forced and natural convection. Computers & Mathematics with Applications, 2011, 61(12): 3585–3592.
[20] Rappaz M, Gandin C A. Probabilistic modelling of microstructure formation in solidification processes. Acta Metallurgica et Materialia, 1993, 41(2): 345–360.
[21] Feng H, Hongshuang D I, Guangshan W. Numerical simulation on solidification microstructure evolution in twin-roll casting process. Hot Working Technology, 2011, 40(5): 57–60. (In Chinese)
[22] Wu S P, Liu D R, Guo J J, et al. Numerical simulation of microstructure evolution of Ti-6Al-4V alloy in vertical centrifugal casting. Materials Science and Engineering: A, 2006, 426(1–2): 240–249.
[23] Wang Q, Wang Y, Li Y, et al. Numerical simulation of the effect of wall-equiaxed crystal density on the number of columnar crystals and the thickness of an equiaxed crystal layer for Al-4.7% Cu alloy ingot based on 3D LBM-CA method. Crystals, 2021, 11(7): 815.
[24] Zhang Z. Numerical simulation of macro segregation during ingot solidification based on mesoscopic scale. Dissertation, Tianjin: Hebei University of Technology, 2018: 71–74. (In Chinese)